applied sciences

MDPI

Article

Modeling and Testing of ESD Protective Textiles

Stanisław Hałgas [1,*], Bożena Wilbik-Hałgas [2] and Piotr Sidyk [1]

[1] Department of Electrical, Electronic, Computer and Control Engineering, Lodz University of Technology, Stefanowskiego 18, 90-537 Lódź, Poland; piotr.sidyk@p.lodz.pl
[2] Institute of Security Technologies MORATEX, Sklodowskiej-Curie 3, 90-505 Lódź, Poland; bhalgas@moratex.eu
* Correspondence: stanislaw.halgas@p.lodz.pl

Featured Application: Protection against electrostatic discharge (ESD) is crucial in many industries and everyday life. The results described in this paper have the potential to be helpful for the design process of ESD textiles. The described modeling process, along with the simulator settings leading to convergent results and the provided plots and illustrations, allow for an understanding of the charge decay phenomenon occurring in textiles.

Abstract: This article discusses the important issue of designing textiles for electrostatic discharge (ESD) protection. ESD protective textiles are used to prevent the failure of electronic circuits. They also safeguard human health and life in explosive environments. The textiles are usually made of woven, knitted, or nonwoven fabrics incorporating a grid or strips of conductive fibers within a base material made of cotton, polyester, or blends of these materials. Various testing standards have been developed to evaluate the suitability of textiles for ESD protection. One of the most widely used is the EN 1149-3 standard, which outlines procedures for recording charge decay plots. The procedure can be used to evaluate all types of textiles. This paper discusses models corresponding to the standard developed in the general-purpose COMSOL Multiphysics software. Using the advanced numerical methods of the software, it is possible to graphically present the phenomena occurring during the application of the standard procedure and to determine the influence of the grid and material parameters on the shape of the charge decay plots. Furthermore, this article compares charge decay plots and shielding effectiveness measured in an accredited laboratory with simulation results.

Keywords: antistatic materials; computer-aided design; electrostatic discharge protection; induction decay method; modeling; shielding effectiveness

check for updates

Citation: Hałgas, S.; Wilbik-Hałgas, B.; Sidyk, P. Modeling and Testing of ESD Protective Textiles. *Appl. Sci.* **2024**, *14*, 7376. https://doi.org/10.3390/app14167376

Academic Editor: Adel Razek

Received: 31 July 2024
Revised: 15 August 2024
Accepted: 16 August 2024
Published: 21 August 2024

Copyright: © 2024 by the authors. Licensee MDPI, Basel, Switzerland. This article is an open access article distributed under the terms and conditions of the Creative Commons Attribution (CC BY) license (https://creativecommons.org/licenses/by/4.0/).

1. Introduction

Electrical charges and discharges are phenomena that occur in everyday life. Electrical discharges (ESDs) can cause dangerous explosions in areas where substances with low ignition energy values are present. ESD also impacts product reliability in every aspect of today's electronic environment. The challenge of protecting electronic systems against ESD energy is present at all stages in the life of electronic hardware, including during manufacturing, storage, delivery, and use. ESD can cause data loss, temporary loss of functionality, or permanent failure. Average product losses due to ESD correspond to between 8 and 33%, and the cost of ESD defects in the electronics industry reaches billions of dollars per year [1]. Improper operator clothing in the production environment leads to approximately 30–50% of all electronic product failures detected during production [2]. Electrical charges are generated during operator movement due to triboelectric effects. Rubbing two textiles against each other can transfer electrostatic charge from one material to the other. If one or both surfaces have low conductivity, the transferred charge remains on the surface after separating them. Almost all synthetic fibers have low humidity and tend to act as insulators, thereby preventing the dissipation of electrostatic charge.

ESD protection is a significant topic in automobile manufacturing plants and the aerospace industry, where a dust-free environment is required [3]. Critical components in power systems, such as cables and circuit boards, often operate at DC voltage. As a result, surface charges are prone to accumulate on the surface of the insulation, resulting in a distorted electric field and triggering electrostatic discharge. ESD is one of the leading causes of severe damage to power equipment and communication systems. Environmental conditions, i.e., air pressure, relative humidity, and temperature, vary according to application area, affecting charge transport and causing difficulties in studying the mechanism of surface discharge [4]. ESD also plays an essential role in the chemical industry and all industries that use filters. Electrical charges accumulated on the walls of a filter can cause hazardous sparks and explosions of flammable substances or combustible dust [5]. Therefore, filters must be designed to dissipate accumulated charges quickly. Small amounts (less than 5%) of conductive fibers randomly distributed in a volume or forming a conductive grid with a grid size of up to a few centimeters allow accumulated charges to be dissipated quickly. However, research is still needed to optimize the nature of the conductive fibers, the amount of conductive fibers used in the felts, and the geometry. Reducing the amount of stainless-steel fibers in a polyester felt by 1% reduces the product's cost by about 20% [6]. A dissertation by Yin [6] focused on the in-depth understanding of charge conduction and dissipation mechanisms on a microscopic scale in antistatic felts and different types of fibers, such as polyester and conductive stainless-steel fibers.

Variable electromagnetic fields produce electromagnetic radiation. Electromagnetic waves are subject to reflection, refraction, diffraction, interference, and absorption. Research focuses on shielding that diffuses or reflects radiation to protect against the harmful effects of radiation. Textile materials can also be used to shield against electromagnetic fields. The shielding effectiveness decreases as the diameter of the metallic wires placed in the fabric increases. Thinner conductive fibers guarantee greater shielding effectiveness. Marciniak et al. [7] presented the results of a study of the shielding effectiveness of a unique hybrid yarn containing a ferromagnetic core and an electrically conductive wire inserted into the fabric.

The current topic in the age of the Internet of Things is the integration of electronic components into conductive textile yarns without compromising textile properties such as flexibility, fit, heat and moisture transfer, and resistance to washing [8–12]. Only products that meet these requirements enable users to accept electronic textiles. A comprehensive review of techniques for integrating conductive materials into and onto textile structures was reported in [9]. Zeng et al. [8], Repon and Mikucionien [10], and Krifa [11] critically reviewed the current state of knowledge concerning the materials, fabrication techniques, and structural designs of devices, as well as applications of fiber-based wearable electronic products, sensors, and antennas. Conductive threads also play a vital role in thermotherapy, where they are used as heating elements to produce the required temperature [13]. They can also improve passenger comfort by incorporating a heating mat made using, for example, distance knitting technology with heating elements into car seats [14].

The effect of ESD is the subject of intensive research. Such studies cover various aspects of yarn, fiber [15,16], and textile manufacturing [1,17,18], as well as antistatic coating and finishing [19–23], modeling [24–27], and testing [24,28–39]. A book by Varnaitė-Žuravliova [40] discusses the significance and fundamental kinds and methods of evaluating antistatic and conductive textiles. The performance of various conductive fibers and the manufacturing of conductive textiles are characterized. ESD research is essential not only in terms of economics but also in the recycling of end-of-life textiles. Natural fibers of plant origin (hemp and flax) and artificial cellulose fibers have the lowest charging tendencies. In contrast, natural fibers of animal origin (wool and natural silk) have a much higher charging abilities. Synthetic and artificial acetate fibers have an incomparably higher charging ability [29]. Industry produces many conductive materials for antistatic and electromagnetic wave-shielding purposes. In most textiles, conductive fibers are mixed with other fibers (natural or synthetic) to provide mechanical properties, mainly elasticity and

tensile strength. There are various ways to prevent problems caused by ESD, including the grounding of all conductive parts, including personnel. Antistatic finishes can reduce static electricity that builds up on the fabric surface. Chemical auxiliaries used to manufacture yarns, knits, fabrics, and nonwoven fabrics also contain antistatic agents.

Both homogeneous and heterogeneous antistatic textiles are available on the market. A homogeneous electrostatic fabric is made of a homogeneous material or a mixture of several different raw materials with slight differences in electrical conductivity. A heterogeneous electrostatic fabric is made of two or more components, one of which is a typical yarn and the other of which is conductive. The difference in electrical conductivity of the components is usually several orders of magnitude. Depending on the required levels of conductivity, geometry, strength, and process requirements, there are different methods for obtaining the desired electrical conductivity of the final product. Conductive yarns can be obtained by adding carbon or metals in various forms, such as wires, fibers, or particles. Conductive polymers can also be used. The textile can also be coated with conductive substances. Specialized textile products, such as dust-free, aseptic, explosion-proof, and antistatic workwear, use organic conductive fibers with high electrical conductivity. Polymers with an intrinsic ability to conduct electricity are also available. Coating conventional textile threads with a layer of conductive polymer allows them to achieve the required electrical conductivity while maintaining the strength and flexibility of the base thread. The main disadvantage of these materials is that they tend to have lower conductivity than metals. Metals such as silver, copper, stainless steel, and aluminum exhibit excellent electrical conductivity within the range of 1.4×10^6 to 63.0×10^6 S/m. Coating fibers with metal results in a highly conductive outer coating. However, long-term wear or repeated laundering usually leads to the degradation of this type of fiber. Twisted stainless-steel yarns are, apart from carbon fibers, most commonly used as conductive fibers. They are characterized by high strength, resistance to oxidation, and very good conductivity compared to metallically coated insulating fabrics. Pure stainless-steel yarns can be woven, knitted, or made into a nonwoven fabric structure. Stainless-steel fibers can be blended with traditional thread, such as cotton or polyester. The disadvantages of stainless-steel yarns are weight and stiffness. In addition to metals, carbon materials such as carbon black, carbon nanofibers, carbon nanotubes, graphite, and graphene can be used in antistatic textiles. From a mechanical point of view, carbon nanotube (CNT) yarns are tensile-resistant, flexible, and lightweight. They have conductivity similar to that of metals and are more oxidation-resistant than stainless steel. Depositing a CNT layer outside of other fibers can also increase conductivity. The main disadvantage of CNT yarns is their cost, which is significantly higher than that of alternatives. Carbon fiber is one of the strongest and lightest materials available today. It is five times stronger and one-third lighter than steel. Carbon fibers are thin strands with a diameter ranging from 5 to 10 μm primarily composed of carbon atoms and possess relatively low electrical conductivity—typically on the order of 100 S/m. However, by adding certain materials, the electrical conductivity of carbon fibers can be increased, leading to values of 10,000 S/m.

ESD protective clothing is usually made of composite fabrics in which a grid or strips of conductive threads are incorporated inside of raw cotton, polyester, or blended materials. Figure 1 shows nonwoven polyester antistatic fabric used to filter various powders, such as dust, cellulose, or chemicals.

ESD protective coats and tunics prevent charging and remove any charge thank to the grid of conductive fibers woven into the fabric. They are worn in medical areas, clean rooms, and hospital laboratories (see Figure 2).

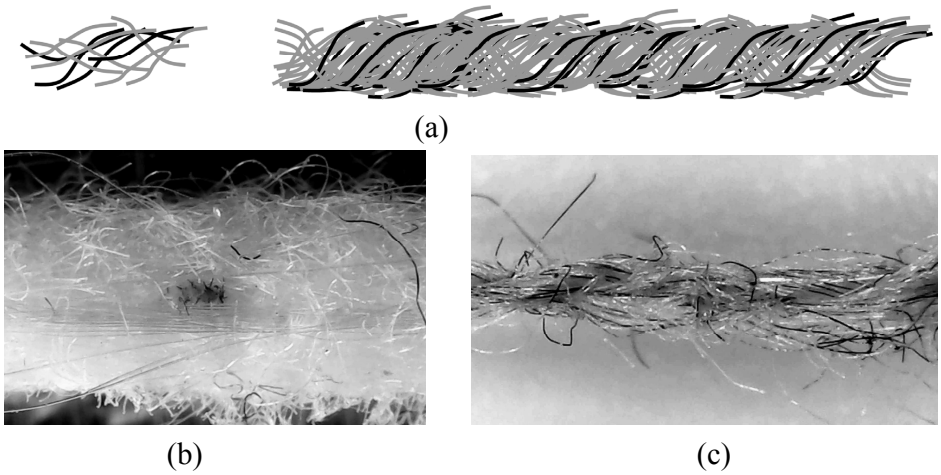

Figure 1. Appearance of polyester/stainless-steel fibers and macroscopic views of a specimen of heterogeneous ESD protective nonwoven polyester antistatic fabric used for the filtering of different powders (conductive fibers in 25 mm × 25 mm grid); (**a**) spun from blend of conductive and nonconductive fibers (drawing [41]); (**b**) cross-section of nonwoven fabric with visible conductive threads; (**c**) polyester/stainless-steel fibers.

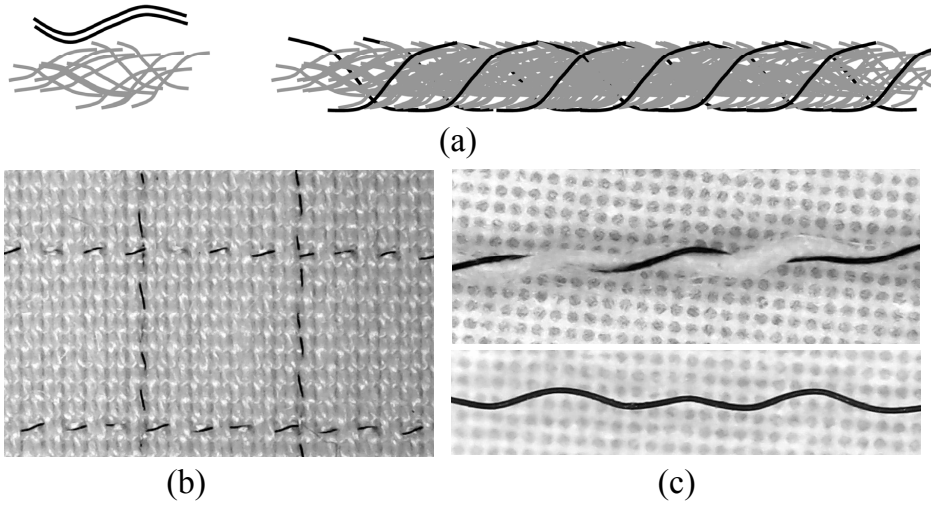

Figure 2. Appearance of carbon-coated fibers and macroscopic views of a specimen of heterogeneous ESD protective fabric made of a combination of 65% polyester, 32% cotton, and 3% carbon-coated fibers (conductive fibers in 5 mm × 5 mm grid); (**a**) spun from conductive fibers and filaments (drawing [41]); (**b**) view of specimen with visible conductive threads; (**c**) polyester/carbon-coated fibers

Reliable textile models must be developed to design protective clothing that meets existing standards for evaluating ESD protective fabrics. This article focuses on modeling fabrics and nonwoven fabrics to determine the charge decay time by induction. Measuring the charge decay time in a material is one of the basic electrostatic tests. The method is suitable for correctly characterizing all types of fabric exposed to ESD. Information about the resistance of conductive fibers can also be deduced from the charge decay plots. The measurement provides information on the effectiveness of the electrostatic shielding of textiles.

The research described in this paper is focused on developing a simplified model of ESD protective textiles with a conductive grid on a 1:1 scale using COMSOL Multiphysics software® [42]. The model allows for the study of how changes in the parameters of the textiles (such as grid size, thickness, and conductivity) affect the charge decay plots following the EN 1149-3 standard [43] (method 2, inductive charging). Simulations make it possible to visualize parts of the charge decay plots that are difficult or impossible to

record under laboratory conditions due to technical limitations. Furthermore, this paper proposes a method for describing the charge decay plots using three exponential terms. Cross-sectional graphs (slices) of the electric field norm allow for a quick evaluation of the electrostatic shielding properties of textiles. Section 2 discusses selected issues related to the testing of ESD protective textiles according to the EN 1149 standard. Section 3 presents the process of modeling textiles in COMSOL Multiphysics® software. The results of numerous simulation studies, some laboratory tests, and a discussion are presented in Section 4. Section 5 contains conclusions.

2. Electrostatic Properties—The Charge Decay Method

The EN 1149 standard [43] specifies test methods for textiles used in producing protective clothing with electrostatic dissipation to prevent incendiary discharge. The standard is divided into test methods for measuring surface resistance (EN 1149-1:2006) [44], vertical resistance (EN 1149-2:1997) [45], and charge decay (EN 1149-3:2004) [43]. The surface resistance is determined along the surface of the material, while the vertical resistance is the electrical resistance perpendicular to the surface. Textile can be conductive ($R_s \leq 10^4\ \Omega$), static dissipative ($10^4 < R_s \leq 10^{10}\ \Omega$), or antistatic ($10^{10} < R_s \leq 10^{11}\ \Omega$) [1]. It has been found that the risk of ESD damage is minimized when the surface resistance of the conductive elements of the garment is within the range of (1×10^5 to $1 \times 10^{11}\ \Omega$) and there are no continuous insulating areas in the garment exceeding a size of about 20 mm × 20 mm [46]. Resistive measurements are often used for qualifying materials where static electricity can cause problems or pose risks. Resistive methods are simple and reliable, especially when the surface resistance of the material under test is less than $1 \times 10^{11}\ \Omega$. In the case of fabrics with a core of conductive fibers, it is impossible to characterize the protective properties of ESD by any resistivity method because the measuring electrode cannot be in galvanic contact with the conductive elements of the textile.

This paper uses the charge decay method to develop a model of two ESD protective textiles, a fabric, and a nonwoven fabric. Charge decay tests are the basis for evaluating antistatic textiles. The EN 1149-3 standard describes two methods of measuring charge decay in detail. The methods differ in the technique of generating electrostatic charge. The first method uses triboelectric charging, while the second uses induction charging. The second method, used during this research, is briefly discussed. It is possible to use a conductor's polarizability to acquire a charge without actually touching a charged object. This process is called charging by induction [47]. The electrification process is not sensitive to surface impurities. The electrostatic induction method utilizes the effect of polarizing a material under exposure to an external electric field. The grounding of the material during the interaction of the field causes a charge to move from the previously electrically neutral material to the ground. The value of the charge depends on the geometry of the system and the value of the electric field intensity (the electric field, in short). The time required to achieve a fully charged state depends on the electrical conductivity (σ) of the material. In the case of metals (high conductivity), the time is on the order of 0.1 ns. For materials with low conductivity, the time is measured in milliseconds. In antistatic materials, charge decay times are usually less than 1 s. The charge decay plot depends, among other things, on the concentration of charge carriers; the mobility of the carriers and the value of the charge (electrical conductivity); the mechanism of charge injection; and the properties of the electrode areas, temperature, and humidity.

Inductive charging involves placing an electrode horizontally under the test specimen (Figure 3). The charge induced on the measuring electrode (2) is the result of the electric field existing in the area of the field-generating electrode (6)—specimen (8)—measuring electrode (2). The field is the result of two components. The first component depends on the field between the measuring electrode (2) and the electrode (6). The second component originates from the charge flowing in from the ground due to the finite conductivity of the material (8) and accumulating on the specimen surface. The charge builds up gradually over time and compensates for the field from the electrode (6). The electrode is left out

of contact with the specimen and is connected to a generator. The generator supplies a step voltage of about 1200 V in 30 µs. A charge of opposite polarity to the electrode is induced on the specimen, which is conductive or contains conductive elements. As a result, the net field is reduced in a manner characteristic of the material under test. The effect is measured and recorded using a field probe (2) and a charge amplifier (1). The EN 1149-3 standard specifies the dimensions of the electrodes and rings and the distances between them. Various textiles (e.g., woven fabrics, warp knits, weft knits, nonwoven fabrics, and laminates), both with and without antistatic components, can be tested and evaluated electrostatically, independent of their structure, using the contactless testing method.

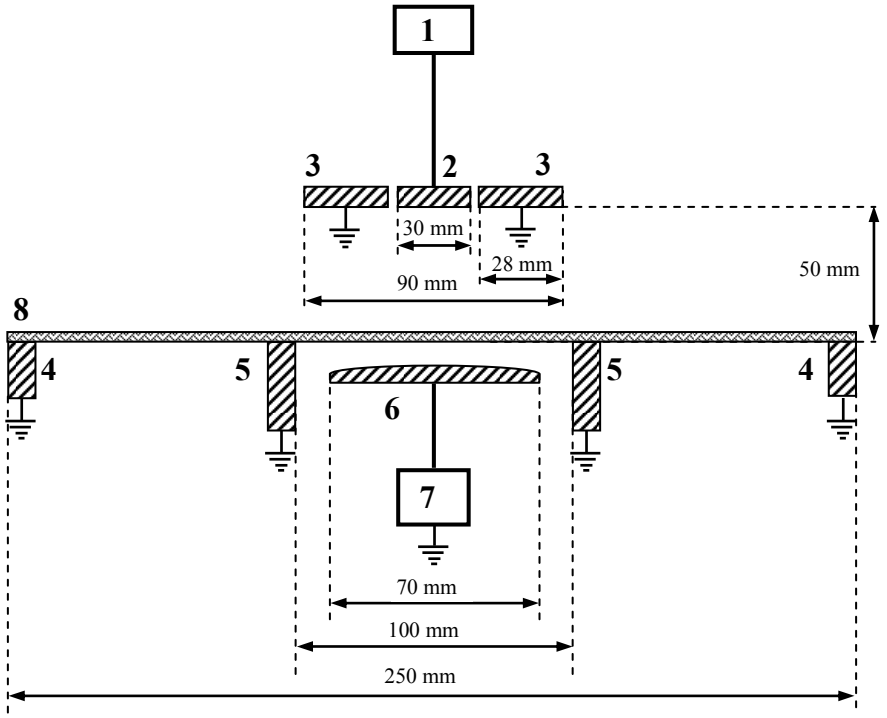

Figure 3. Overview diagram of inductive charging test method; 1—charge amplifier and recording device; 2—field measuring probe; 3—guard ring; 4—specimen clamping ring; 5—support ring; 6—field electrode; 7—voltage generator; 8—test specimen

A control measurement is first performed without a specimen between the field electrode and the measuring probe. The measuring probe indicates a fixed maximum value (E_{max}). Next, a measurement is performed with the specimen. After the specimen is clamped, a static neutralizer removes any residual static charge. The test probe indicates a value of zero or close to zero. A step voltage is applied from the voltage generator to the field electrode. The recording device is stopped when the measurement probe reading drops to at least half of the maximum value or after 30 s—whichever comes first. Let E_R be the maximum electric field indicated on the recording device with the test specimen in the measuring position. The values of E_R and t_{50} are recorded. The plot shown in Figure 4a corresponds to materials with no shielding effect. The plot can span time intervals from hundreds of milliseconds (for antistatic materials) to even years (for good electrets). The discharge time dependence of a homogeneous material can be approximately described by the following equation:

$$E(t) = E_{max} \times \mathrm{e}^{-t/(RC)} \quad (1)$$

where E_{max} is defined as above, C is the capacitance, R is the resistance of the specimen, and t is time [48]. For materials with shielding effects, E_R is less than E_{max} (see Figure 4b). Peaks occurring at the beginning are ignored when calculating E_R. If $E_R < E_{max}/2$, t_{50} is

recorded as less than 0.01 s. If the indicated field has not decayed to $E_{max}/2$ within 30 s, t_{50} is recorded as greater than 30 s [43,48]. The E_R point determines the transition of the fast discharge through the conducting fiber into the slow discharge of the base fabric (e.g., polyester). The E_R/E_{max} ratio depends on the grid density of the conducting fibers in the textile and is called field penetration. For small spacing between the conducting fibers, $E_R/E_{max} \to 0$. Based on the ratio E_R/E_{max}, the value of the electrostatic shielding S can be determined,

$$S = 1 - \frac{E_R}{E_{max}}. \quad (2)$$

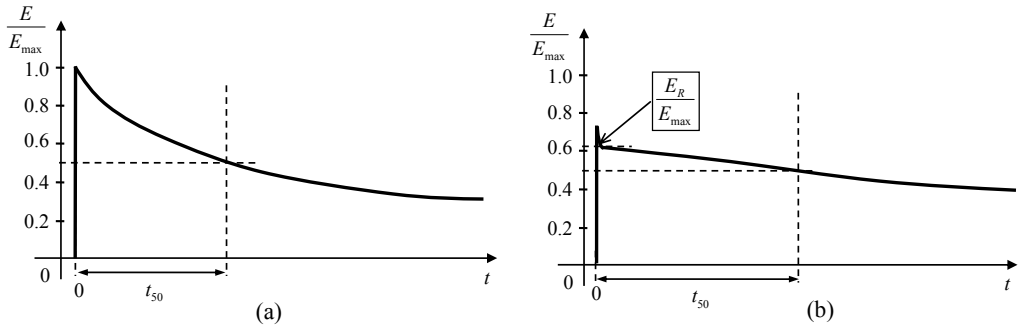

Figure 4. Exemplary plots of charge decay measurement records (sketches). (**a**) Dissipative material without shielding effect; (**b**) dissipative material with shielding effect.

3. Modeling of ESD Textiles in General-Purpose Multiphysics Software

Several software environments are available for the modeling of complex physical problems, such as Ansys [49], CST Studio Suite® [50], and COMSOL Multiphysics® [42]. In this paper, COMSOL software is used. The software offers fully coupled capabilities for multiphysics modeling. It allows for control of the flow of the numerical process by selecting methods of numerical integration and solving linear and nonlinear algebraic equations. The simulation's data management, export ability, and graphics are also very advanced.

Developing reliable models to design protective textiles that meet existing standards for the evaluation of electrostatic discharge is necessary. The problem is very complex because the diameters of the conductive threads are small relative to the dimensions of the specimen and test stand, and the electrical conductivities of the base and conductive materials differ by up to several orders of magnitude. Hałgas and Wilbik-Hałgas [27] focused on modeling fabrics to determine surface and vertical resistance. They used sophisticated modeling at the thread level, with an average electrical conductivity value for the conductive yarn. The analysis used the cooperation of electrical current and electrical circuit modules. The developed model is very complex, so the analysis time is long. However, due to the measuring electrodes' dimensions and the static analysis, the model proved to be a good starting point for the development of simplified circuit models.

This article focuses on modeling fabrics and nonwoven fabrics to determine charge decay times by induction. Measuring the charge decay time in a textile is one of the basic electrostatic tests and can be used to characterize all types of fabrics exposed to ESD. The models proposed in this paper can be applied to the design of textiles according to the EN 1149-3 standard. The electrodes and the specimen are much larger for the test than for tests in which surface and vertical resistances are determined. Moreover, the test itself leads outputs characteristics versus time. Thus, the model must be significantly simplified to obtain results in an acceptable time.

Three-dimensional electromagnetic models of the electrode (6) and rings (3, 4, and 5) (see Figure 3) were developed on a 1:1 scale in the electric currents module. The geometry of the electrodes and the distances on the laboratory bench comply with the technical conditions presented in the EN 1149-3 standard. A probe (point probe) was placed in the center of the ring (3) instead of the measuring electrode. The probe collects the electric field norm over time. The specimen (8) is modeled using a cylinder with a radius of 128 mm

and a thickness corresponding to the actual specimen. Relative permeability and electrical conductivity parameters of the cylinder correspond to the base textile material (polyester, polyamide, or cotton), taking into account any treatment (e.g., singeing/firing (a process whereby the textile is passed over an open flame or heated plates to burn off protruding fibers on the surface; this results in a smoother fabric with an improved appearance and reduced pilling) or impregnation). A grid of conductive fibers is placed in the middle of the thickness of the cylinder. Preliminary studies have shown that such grid placement avoids many problems in numerical meshing. In addition, as verified in many other models with higher accuracy but smaller geometric dimensions, direct contact of the conductive thread with the rings does not significantly affect the results obtained with textiles less than 3 mm thick. The cross-section of the grid elements is rectangular, with dimensions as close to the actual measurements as possible. Such a grid is easily generated using the difference operation in COMSOL. An electrical potential of 1200 V is applied to the field electrode (6). Next, a mesh sequence with two free triangular nodes is created. The analysis time is set in the range of 0 to 30 s (if not specified otherwise), with a step of 100 ms (if not specified otherwise). The problem's complexity is due to the significant difference in the conductivity of the base material and the conductive thread. Adjusting the solver settings is necessary. The problem is solved using a coupled direct solver. Newton (automatic) is selected as the nonlinear method, the maximum number of iterations is set to 30, and the relative tolerance is 0.01. In addition to plotting the electric field norm over time, cross-sectional plots (slices) of the electric field norm in different planes are found. Calculations were performed on a computer with an Intel Core i7-6700 processor and 64 GB of RAM.

4. Results and Discussion

This section discusses the different steps of textile simulation corresponding to the tests according to the EN 1149-3 standard. In addition, test results for two ESD textiles from an accredited laboratory are presented. The same color scale (with a manual color range from 0 to 50,000 V/m) is used for all the slice diagrams in the simulation. The darkest blue color represents the minimum electric field norm (0 V/m), while the darkest red represents values of 50,000 V/m and above.

4.1. Determination of the Maximum Value of the Electric Field Norm

A model was built to determine the maximum value of the electric field norm at the point probe without any specimen. The mesh of the model is shown in Figure 5a. The simulation resulted in E_{max} equal to 6440 V/m. Figure 5b shows the slice plot for a cross-section in the $y - z$ plane passing through the model's center point. Figures 5c–e show the slice plot in the $x - y$ plane for three z coordinates corresponding to distances (d) of 0.1 mm, 1 mm, and 2 mm from the plane determined by rings (4) and (5) in Figure 3 (which corresponds to the bottom surface of the specimen (8)).

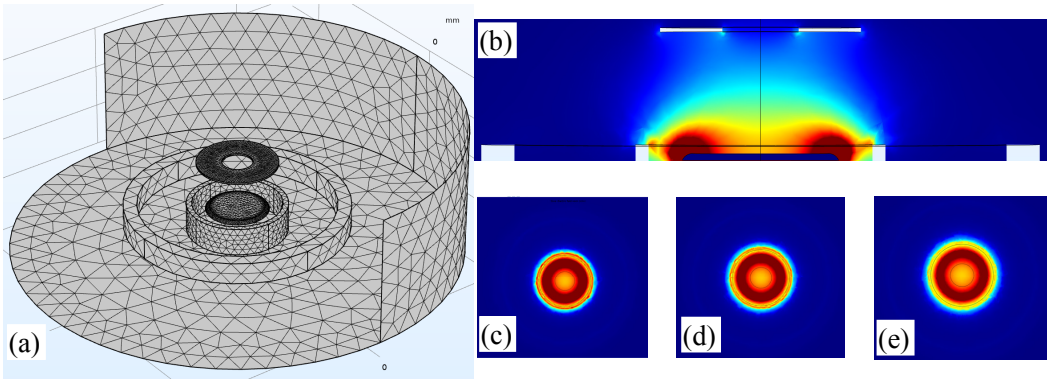

Figure 5. Meshing results (**a**) and slice plots for the model to determine E_{max} (**b**–**e**);slice in the $y - z$ plane for $t = 0$ s (**b**) ; slices in the $x - y$ plane for $d = 0.1$ mm and $t = 0$ s (**c**), $d = 1$ mm and $t = 0$ s (**d**), $d = 2$ mm and $t = 0$ s (**e**).

4.2. Charge Decay Plots for Homogenous Textiles

The effect of the electrical conductivity of the raw material in the ESD protective textile on the charge decay plots was considered. For this purpose, a model was built, and the mesh shown in Figure 6a was generated. A specimen thickness of 1.8 mm was assumed (corresponding to the thickness of the nonwoven fabric tested in the laboratory). Simulations were carried out for conductivity (σ) from the set of $\{1 \times 10^{-13}, 1 \times 10^{-12}, 1 \times 10^{-11}, 3 \times 10^{-11}, 1 \times 10^{-10}\}$, all in S/m. Figure 6b–m show slice plots for $\sigma = 3 \times 10^{-11}$ S/m. Figure 6b shows the slice in the $y - z$ plane crossing the model midpoint for $t = 0$ s, and Figure 6c depicts $t = 15.7$ s, which corresponds to t_{50} in the EN 1149-3 standard. Figure 6d–m show slices in the $x - y$ plane for five values of the z coordinate corresponding to distances (d) of 0.1 mm, 1 mm, 2 mm, 5 mm, and 50 mm from the bottom surface of the specimen at $t = 0$ s, and $t = 15.7$ s. Figure 7 shows the charge decay characteristics for all assumed conductance values. It can be seen that at a fixed specimen thickness, $t_{50} < 30$ s can be determined only for conductivities of 3×10^{-11} S/m and 1×10^{-10} S/m (curves (d) and (e)). For a conductivity value of 1×10^{-10} S/m, the time is 4.3 s, slightly exceeding the 4 s allowed by the standard.

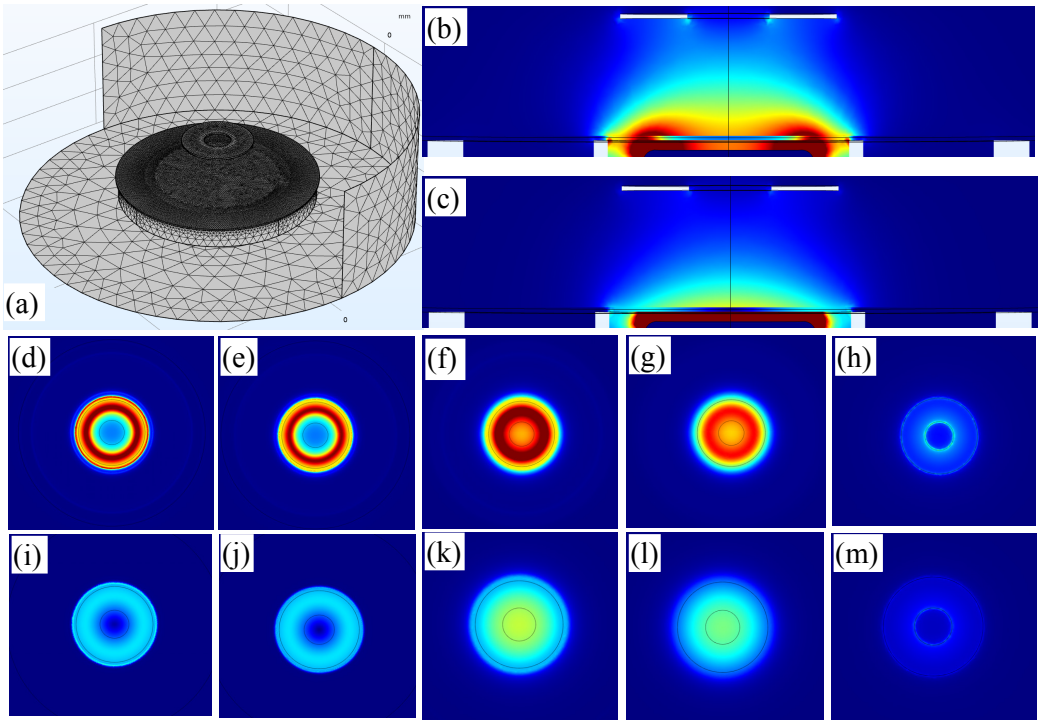

Figure 6. Meshing result (**a**) and slice plots for specimen with a textile conductivity of $\sigma = 3 \times 10^{-11}$ S/m (**b**–**m**); slices in the $y - z$ plane for $t = 0$ s (**b**) and $t = 15.7$ s (**c**); slices in the $x - y$ plane for $d = 0.1$ mm and $t = 0$ s (**d**), $d = 1$ mm and $t = 0$ s (**e**), $d = 2$ mm and $t = 0$ s (**f**), $d = 5$ mm and $t = 0$ s (**g**), $d = 50$ mm and $t = 0$ s (**h**), $d = 0.1$ mm and $t = 15.7$ s (**i**), $d = 1$ mm and $t = 15.7$ s (**j**), $d = 2$ mm and $t = 15.7$ s (**k**), $d = 5$ mm and $t = 15.7$ s (**l**), and $d = 50$ mm and $t = 15.7$ s (**m**).

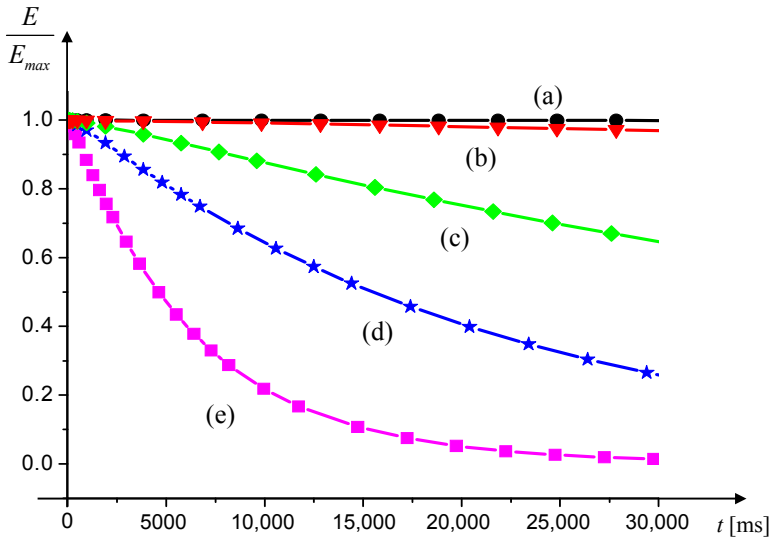

Figure 7. Charge decay plots for textile with a thickness of 1.8 mm (result of simulations). (**a**) $\sigma = 1 \times 10^{-13}$ S/m; (**b**) $\sigma = 1 \times 10^{-12}$ S/m; (**c**) $\sigma = 1 \times 10^{-11}$ S/m; (**d**) $\sigma = 3 \times 10^{-11}$ S/m; (**e**) $\sigma = 1 \times 10^{-10}$ S/m.

4.3. Simulation for Nonwoven Antistatic Fabric

The first ESD protective textile studied by simulation was nonwoven antistatic fabric. The thickness of the material was assumed to be 1.8 mm, and the conductive grid was 25 mm × 25 mm. The conductive thread was assumed to have a rectangular cross-section of 0.5 mm × 0.25 mm. The effects of the conductivity of the base material and the conductivity of the conductive fibers on the charge decay plots were investigated. The mesh of the model is shown in Figure 8a. Simulations were carried out for base-material conductivities (σ_1) from the set of $\{1 \times 10^{-13}, 1 \times 10^{-12}, 1 \times 10^{-11}, 3 \times 10^{-11}, 1 \times 10^{-10}\}$ and for conductive fiber conductivities (σ_2) from the set of {17,500, 10,000, 100, 10, 1, 0.01, 0.0001, and 0.000001}, all in S/m. Figure 8b shows an exemplary slice plot in the $y - z$ plane crossing the model midpoint for $t = 100$ ms, $\sigma_1 = 3 \times 10^{-11}$ S/m, and $\sigma_2 = 1$ S/m. Figure 8c–e show slices for the same parameters in the $x - y$ plane for three values of the z coordinate corresponding to distances (d) of 0.1 mm, 1 mm, 2 mm from the bottom surface of the specimen. Figure 9 shows the charge decay plots for all assumed conductivities of the base materials.

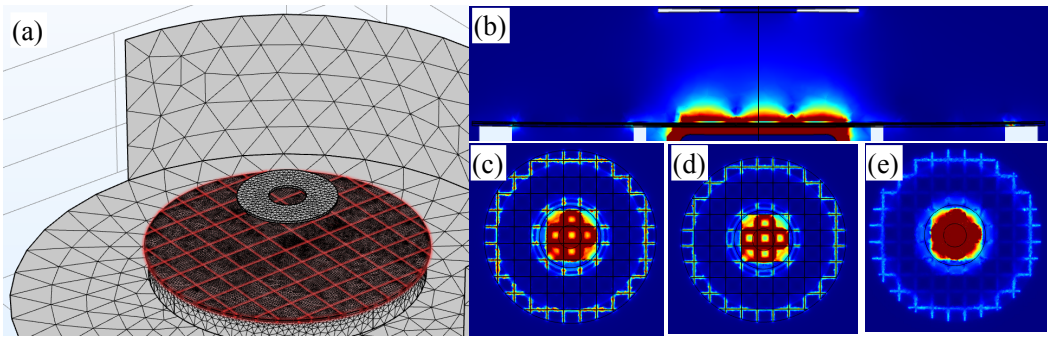

Figure 8. Meshing result (**a**) and slice plots (**b**–**e**) for nonwoven antistatic fabric with parameters of $\sigma_1 = 3 \times 10^{-11}$ S/m and $\sigma_2 = 1$ S/m at $t = 100$ ms; the slice in the $y - z$ plane (**b**); and the slices in the $x - y$ plane for $d = 0.1$ mm (**c**), $d = 1$ mm (**d**), and $d = 2$ mm (**e**).

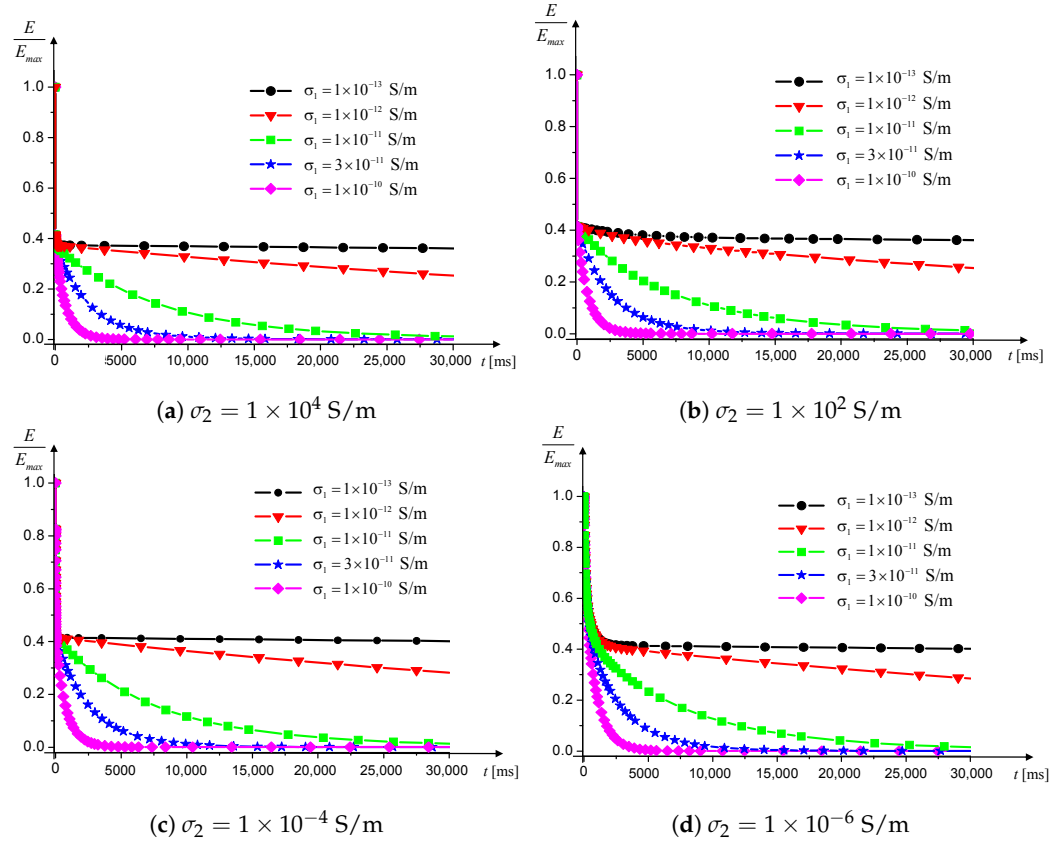

(**a**) $\sigma_2 = 1 \times 10^4$ S/m (**b**) $\sigma_2 = 1 \times 10^2$ S/m

(**c**) $\sigma_2 = 1 \times 10^{-4}$ S/m (**d**) $\sigma_2 = 1 \times 10^{-6}$ S/m

Figure 9. Charge decay plots for a textile thickness of 1.8 mm (result of simulations).

The t_{50} for all $\sigma_2 > 1 \times 10^{-6}$ S/m is below 0.01 s for all base material conductivity values. For $\sigma_2 = 1 \times 10^{-6}$ S/m, t_{50} is about 530 ms for $\sigma_1 = 1 \times 10^{-13}$ S/m and $\sigma_1 = 1 \times 10^{-12}$ S/m, 500 ms for $\sigma_1 = 1 \times 10^{-11}$ S/m, 380 ms for $\sigma_1 = 3 \times 10^{-11}$ S/m, and 300 ms for $\sigma_1 = 1 \times 10^{-10}$ S/m. Thus, all the textiles meet the EN 1149-3 standard. To provide further insight into the results, plots were also created for a fixed σ_1 and four values of σ_2 (10,000, 100, 0.0001, and 0.000001, all in S/m) (Figure 10).

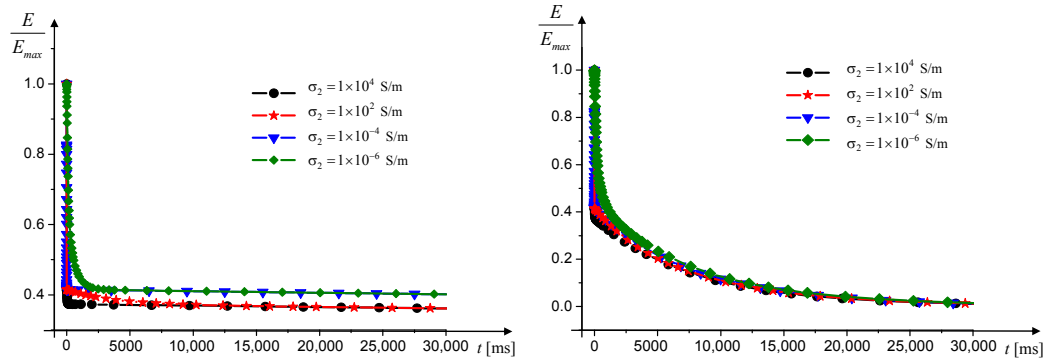

(**a**) $\sigma_1 = 1 \times 10^{-13}$ S/m (**b**) $\sigma_1 = 1 \times 10^{-11}$ S/m

Figure 10. *Cont.*

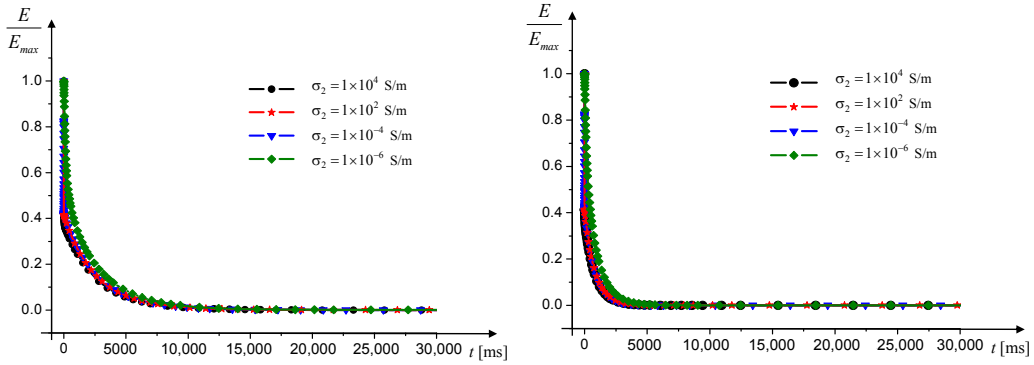

(**c**) $\sigma_1 = 3 \times 10^{-11}$ S/m (**d**) $\sigma_1 = 1 \times 10^{-10}$ S/m

Figure 10. Charge decay plots for a textile thickness of 1.8 mm (result of simulations).

Most plots show a rapid decay of the electric field norm from the maximum (or near-maximum) value to E_R. The time of this decay for large σ_2 values is a fraction of nanoseconds. Therefore, it is necessary to run simulations with a tiny step near zero to illustrate this phenomenon. For $\sigma_1 = 1 \times 10^{-13}$ S/m and $\sigma_2 = 10,000$ S/m, the analysis time should be 0 to 1 ns with a step of 1 ps. Figure 11 depicts the change in electric field norm over a time window of 0 to 200 microseconds for $\sigma_1 = 3 \times 10^{-11}$ S/m and $\sigma_2 = 0.01$ S/m, revealing the expected exponential nature of the charge decay. Figure 12 shows slice plots in the $y - z$ plane for 16 time points. After about 1 microsecond under the parameters of the base material and conductive grid, the first effects of the grid on the electric field can be seen. The shielding effect and a decrease in the electric field norm at the point probe can be observed with increasing time. Figure 13 shows slice plots in the $x - y$ plane 2 mm away from the bottom surface of the specimen for the same 16 time points.

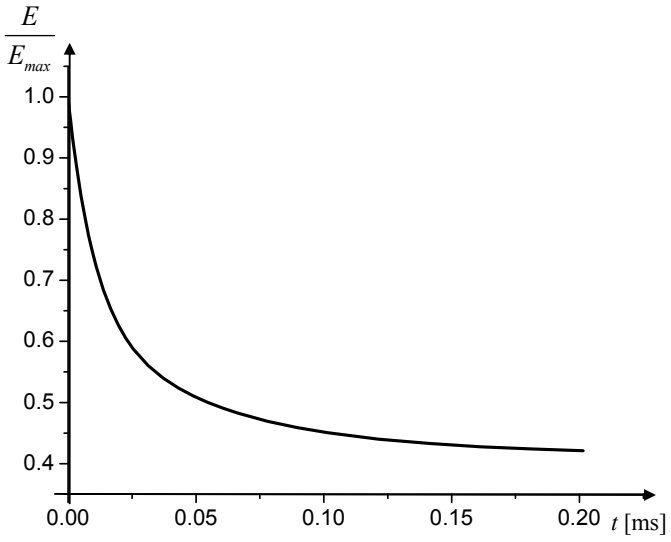

Figure 11. Charge decay plots for a textile thickness of 1.8 mm, $\sigma_1 = 3 \times 10^{-11}$ S/m, and $\sigma_2 = 0.01$ S/m (result of simulation).

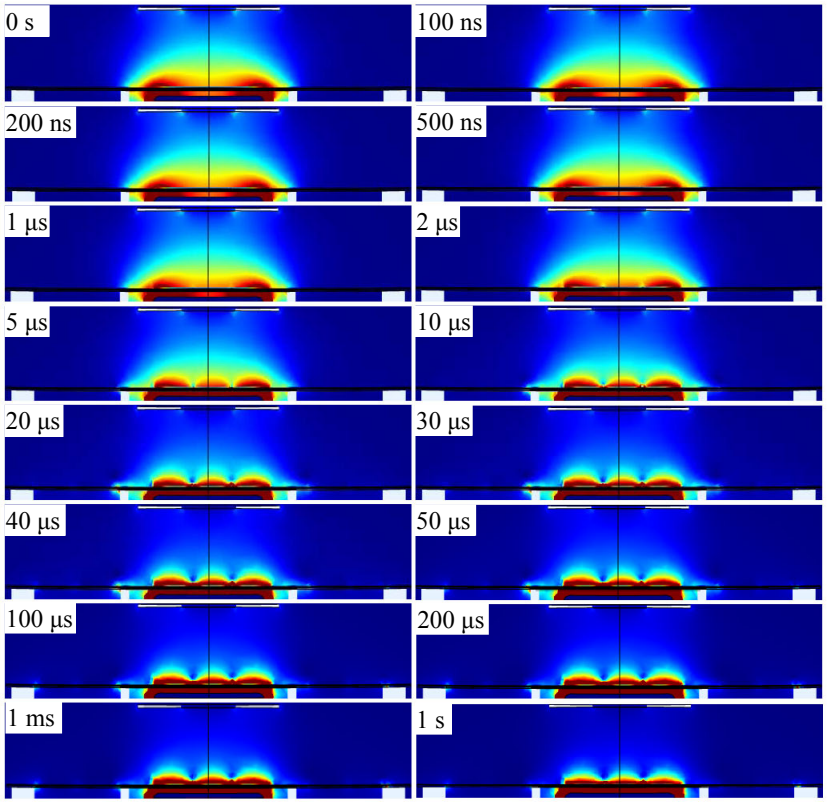

Figure 12. Slice plots in the $y-z$ plane for $\sigma_1 = 3 \times 10^{-11}$ S/m, $\sigma_2 = 0.01$ S/m, and 16 time points.

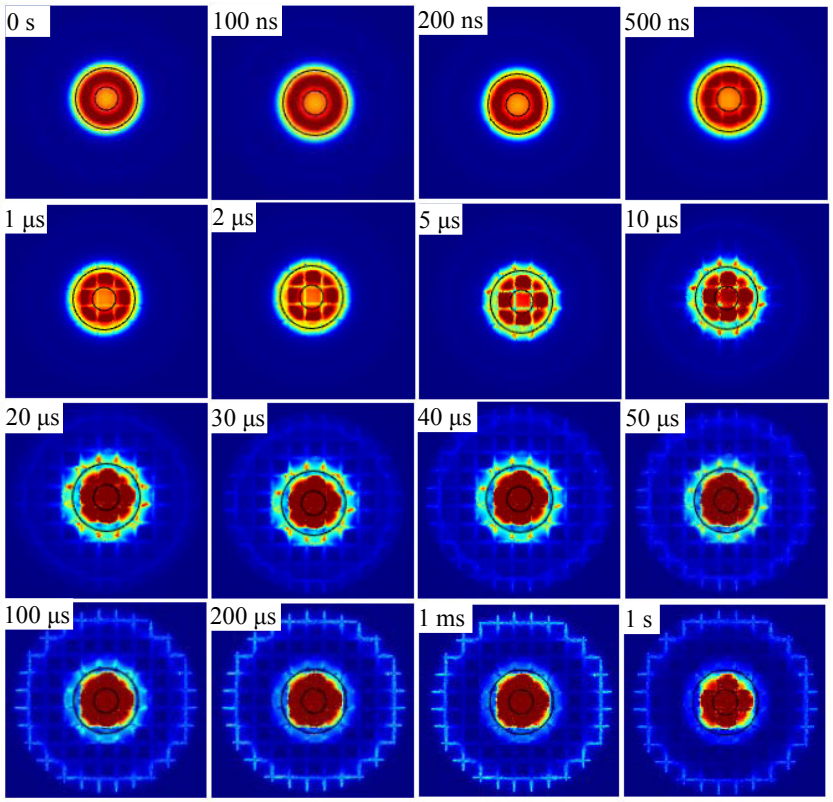

Figure 13. Slice plots in the $x-y$ plane 2 mm away from the bottom surface of the specimen for $\sigma_1 = 3 \times 10^{-11}$ S/m, $\sigma_2 = 0.01$ S/m, and 16 time points.

4.4. Simulation for ESD Protective Fabric

The second textile tested was a polyester fabric with a conductive grid. The thickness of the material was assumed to be 0.35 mm, and the conductive grid was 5 mm × 5 mm. The conductive fiber was assumed to have a square cross-section of 0.02 mm × 0.02 mm. This model is much more complex than the model considered in the previous section, and the analysis time is also much longer. Figure 14a shows the model's meshing effect, and Figure 14b shows an enlarged part of the mesh. Simulations were performed for a base-material conductivity of $\sigma_1 = 1 \times 10^{-13}$ S/m (a typical conductance for polyester) and conductive-fiber conductivities of $\sigma_2 = 100$ S/m (a typical conductance for carbon threads) and $\sigma_2 = 0.001$ S/m.

Figure 15 shows the charge decay plots for the assumed conductivities. The time at t_{50} is below 0.01 s. Thus, the textiles meet the EN 1149-3 standard. Figures 16 and 17 show slice plots for several time points in the $x - y$ and $y - z$ planes. Analysis of the figures suggests that the fabric effectively shields against electric fields.

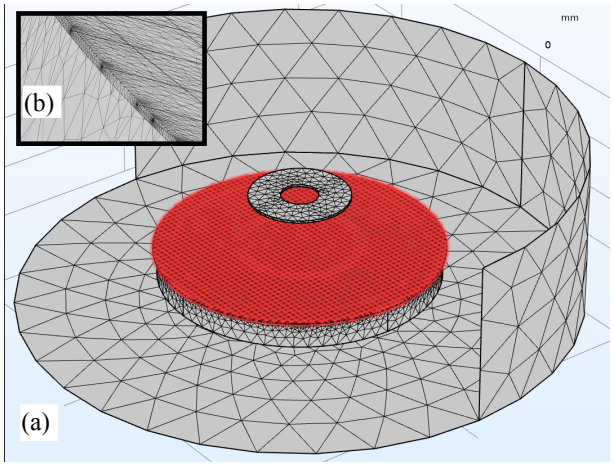

Figure 14. Meshing result of the polyester fabric model. (**a**) Full model; (**b**) an enlarged part of the model.

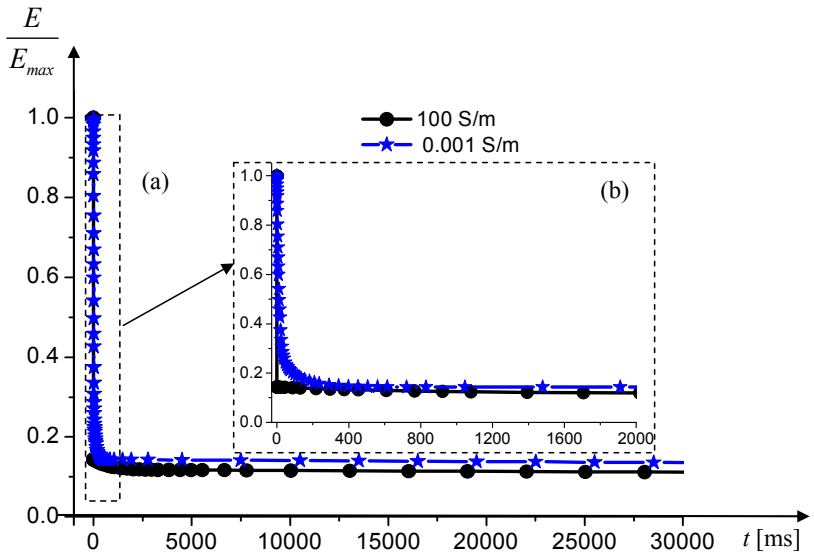

Figure 15. Charge decay plots for a textile thickness of 0.35 mm and $\sigma = 1 \times 10^{-13}$ S/m (result of simulations); (**a**) the full scale; (**b**) the zoomed initial part of the plot.

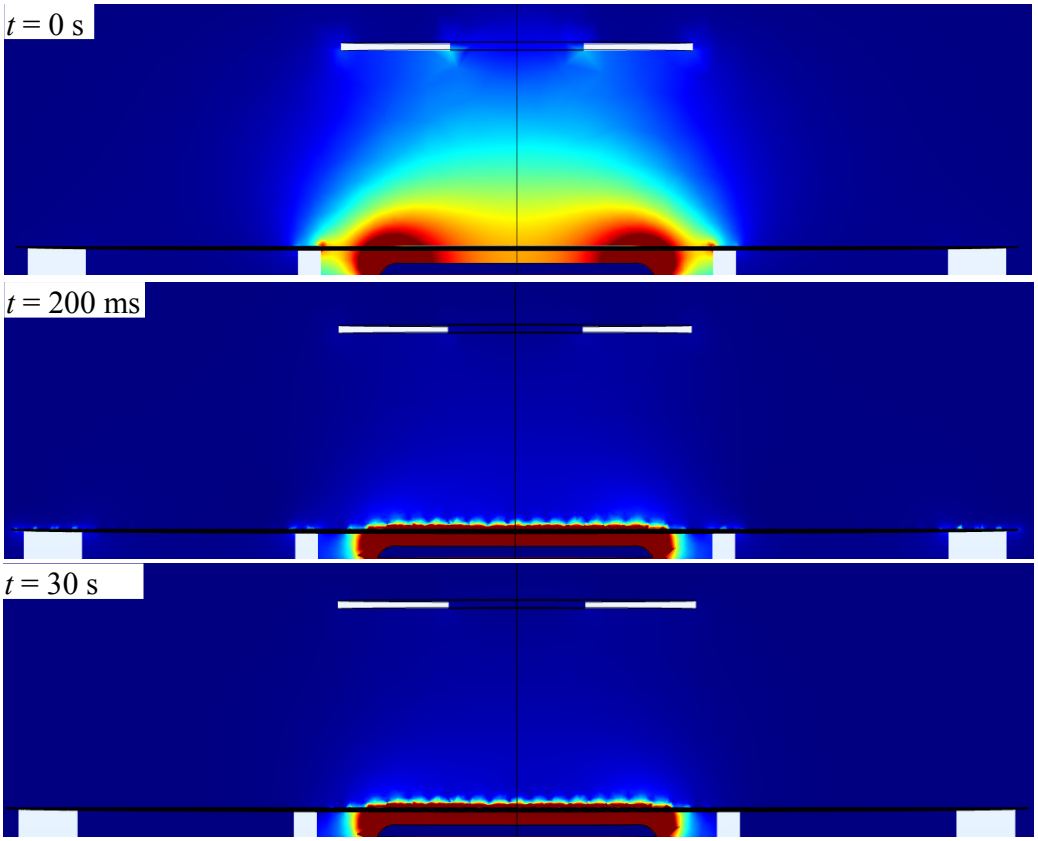

Figure 16. Slice plots in the $y - z$ plane for a textile thickness of 0.35 mm with parameters of $\sigma_1 = 1 \times 10^{-13}$ S/m and $\sigma_2 = 100$ S/m at three time points.

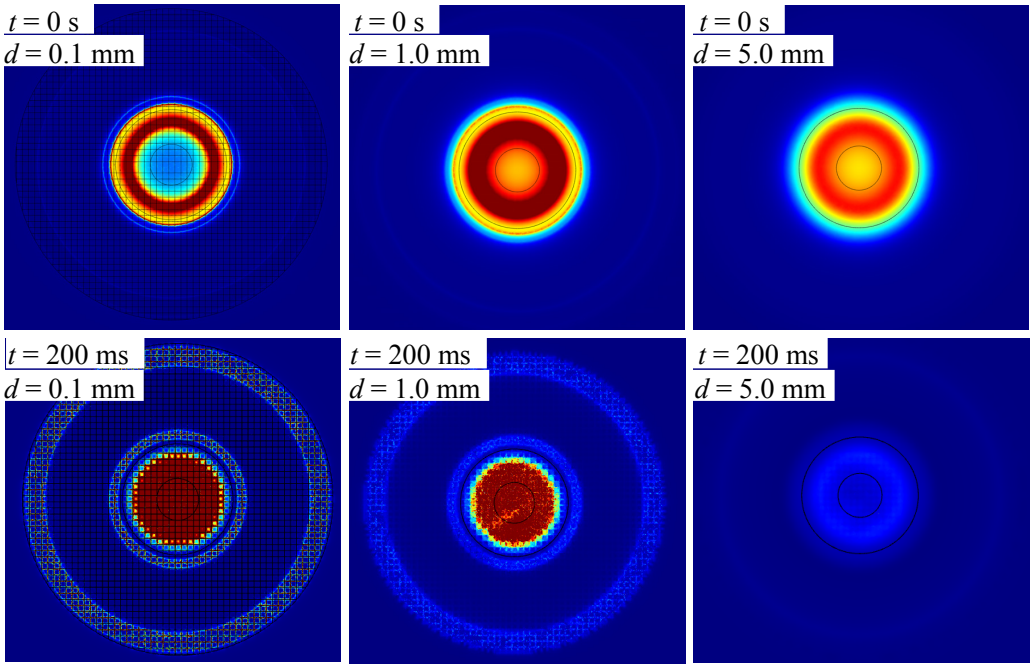

Figure 17. Slice plots in the $x - y$ plane for a textile thickness of 0.35 mm and parameters of $\sigma_1 = 1 \times 10^{-13}$ S/m and $\sigma_2 = 100$ S/m at two time points and three distances (d) from the bottom surface of the specimen.

4.5. Laboratory Tests

Both textiles shown in Figures 1 and 2, i.e., the protective nonwoven fabric and ESD protective fabric, were tested in an accredited laboratory. The nonwoven fabric is made of polyester fibers (3.6 dtex) placed in random directions and has internal cohesion ensured by a mechanical method. The grid of conductive fibers is embedded. Additionally, the felt was fired and impregnated with an oleo-hydrophobic substance. The fabric shown in Figure 2 is a plain-weave fabric made of 9 tex x2 polyester/cotton fibers and 12 tex polyester/carbon-coated fibers. The most important information and parameters of the tested textiles are included in Table 1.

Table 1. Comparison of the experimental subjects.

No. of textile	1	2
Type of textile	nonwoven fabric (felt)	fabric
Thickness of textile	1.8 mm	0.35 mm
Material composition	98% polyester 2% stainless steel	60% polyester 37% cotton 3% carbon-coated yarn
Density	266 kg/m^3	380 kg/m^3
Conductive grid	25 mm × 25 mm	5 mm × 5 mm
Diameter of conductive fiber	0.42 mm	0.022 mm
Type of conductive yarn	blend of polyester and stainless-steel fibers	carbon-coated fiber twisted with polyester fibers

During laboratory tests, a measurement device was used to determine charge decay time (Figure 18a). The device was connected to a laptop with dedicated software installed to control the measurement process. The key parameters of the setup are as follows: time resolution of 50 µs (sampling frequency 20 kHz), a charge amplifier (electronic electrometer) with a range of 1 pC to 2 nC, 16-bit measurement resolution, input impedance of 1 GΩ, and rise time of 0.2 V/µs. The laptop used during the test was running on battery power, and the measurement setup was powered on for 10 min before the test began. The setup was located in a Binder Climate Chamber KBF 240, Binder, Tuttlingen, Germany. The tests were conducted in accordance with the steps outlined in the EN 1149-3 standard using three textile specimens. The test procedure involves the following steps:

1. Cutting three specimens (each at least 300 mm square, excluding seams);
2. Determining the initial maximum field strength without a specimen (E_{max});
3. Conducting the following measurements with the specimen:
    - Clamping the first test specimen in the clamping ring;
    - Removing any residual electrostatic charge using the static neutralizer (Figure 18b);
    - Initiating the measurement and noting E_R and t_{50}; (Figure 18c)
    - Removing the specimen and repeating the procedure with the remaining two specimens.
4. Calculating the mean values of the half decay time (t_{50}) and the shielding factor (S).

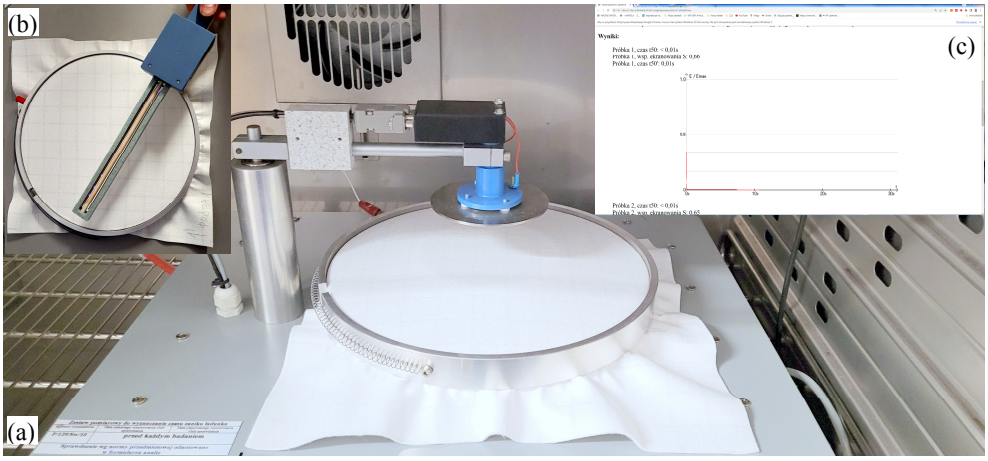

Figure 18. Photo of the laboratory bench. (**a**) Nonwoven fabric specimen placed in the terminals of the charge decay instrument; (**b**) residual charge neutralizer moved over the specimen; (**c**) the obtained results.

Charge decay plots were recorded, and the time (t_{50}) and electrostatic shielding value (S) were determined for three specimens of each textile under two climatic conditions (at 23 °C and 25% relative humidity (RH); 28 °C and 52% RH). In the case of a nonwoven fabric made of polyester fibers and a conductive grid using stainless-steel fibers, the nonwoven textile was additionally fired and treated with oleo-hydrophobic impregnation. The additional pretreatment positively impacts the antistatic properties, significantly increasing the effective electrical conductivity by about three orders of magnitude compared to untreated nonwoven polyester fabric. The time (t_{50}) is less than 0.01 s for all specimens under all climatic conditions. For the nonwoven fabric under the climatic conditions established in the 1149-3 standard, the average value of S equals 0.61, and at 28 °C and 52% RH, the average value equals 0.66. As expected, at higher humidity, the conductivity of the specimen increases, and oleophobic impregnation enhances the effect. Figure 19 shows the charge decay plot for nonwoven fabric under standard climatic conditions. For ESD protective fabric under standard climatic conditions, an average value of $S = 0.97$ is obtained. At 28 °C and 52% RH, the average value of S equals 0.98. Figure 20 shows the charge decay plot for the fabric under standard climatic conditions.

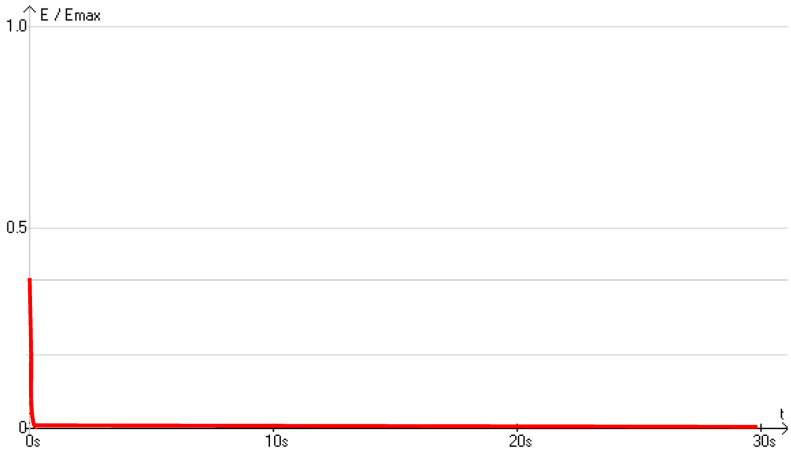

Figure 19. Charge decay plots for nonwoven polyester antistatic fabric at 23 °C and 25% RH measured in a laboratory.

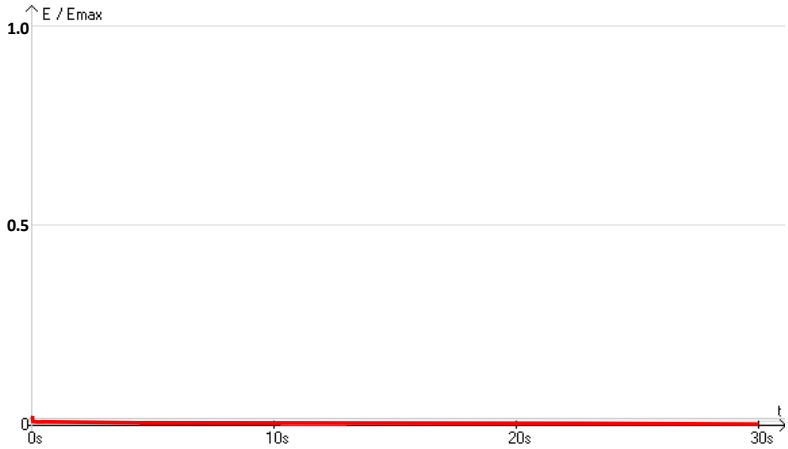

Figure 20. Charge decay plots for ESD protective fabric at 23 °C and 25% RH measured in a laboratory.

4.6. Discussion

The developed simplified model of ESD protective textiles allows us to carry out a preliminary design of textiles that meet the requirements of the EN 1149-3 standard. Slice plots not previously presented in the literature illustrate the electric field shielding by such textiles. Based on the plots shown in Figures 9 and 10 (or the corresponding tabular data), the S parameter, determined by Equation (2), is easy to find. For conductive fibers with $\sigma_2 > 0.0001$ S/m, the parameter almost does not depend on the value of σ_1. For example, for the curves in Figure 9a, the S parameter equals 0.62, and for the curves in Figure 9c, $S = 0.59$. Additional analyses of the time just after switching on the electrode power supply allow for the plotting of charge decay plots usually not observed during laboratory tests due to the sampling time of the output signal (see Figures 19 and 20). From Figures 9 and 10, it can be seen that regardless of the conductivity of the conductive fibers (σ_2), the curves at $\sigma_1 < 1 \times 10^{-13}$ S/m run almost horizontally for $t > 10$ s. In fact, they very slowly and exponentially tend to zero. Such σ_1 values correspond, for example, to polyester textiles without additional treatment of the final product (impregnation and firing). Analyzing the measurement outcome shown in Figure 19, it can be seen that the most similar characteristics, with the same S, are obtained for the model considered in Section 4.3 at $\sigma_1 = 1 \times 10^{-9}$ S/m and $\sigma_2 = 17,500$ S/m (see Figure 21). Although the base material is polyester, the conductivity of the material is reduced to $\sigma_1 = 1 \times 10^{-9}$ S/m by firing and impregnation. The absence of these steps would lead to the characteristics shown in Figure 9a at $\sigma_1 = 1 \times 10^{-13}$ S/m.

Changes in the parameters of the textiles, particularly the thickness and conductivity of the base material and the conductive fibers within a range of up to 10%, do not cause significant changes in the shape of the charge decay plots. The curves practically overlap on the 0–30 s scale. Parametric studies can be carried out in the COMSOL environment. With a high-performance computer. families of charge decay plots can be found to determine the manufacturer's required textile manufacturing tolerances. However, due to the type of basic analysis performed (transient analysis), the time consumption of the process is very long. Some additional simulations were carried out to highlight the tolerance problem. A nonwoven fabric (felt) with nominal thickness values of 1.8 mm, $\sigma_1 = 1 \times 10^{-11}$ S/m, and $\sigma_2 = 1 \times 10^{-6}$ S/m was considered. For nominal parameters, t_{50} equals 480 ms. Changing the thickness to 1.62 mm and 1.98 mm hardly changes the time. A 10% change in σ_1 results in a 1% change in t_{50}, while a 10% change in σ_2 leads to around an 8% change in t_{50}. The occurrence of areas of non-uniform final treatment (impregnation and firing) in textiles can significantly affect local ESD protection properties. Such defects in textiles are, however, difficult to predict and model. In the testing process, according to the EN 1149-3 standard, if such a defect is only local and is not repeated across the whole material surface, tests on different specimens can identify such heterogeneity. Of course, the model can be

extended to include heterogeneity, but the results can only have a cognitive significance due to the randomness of such defects.

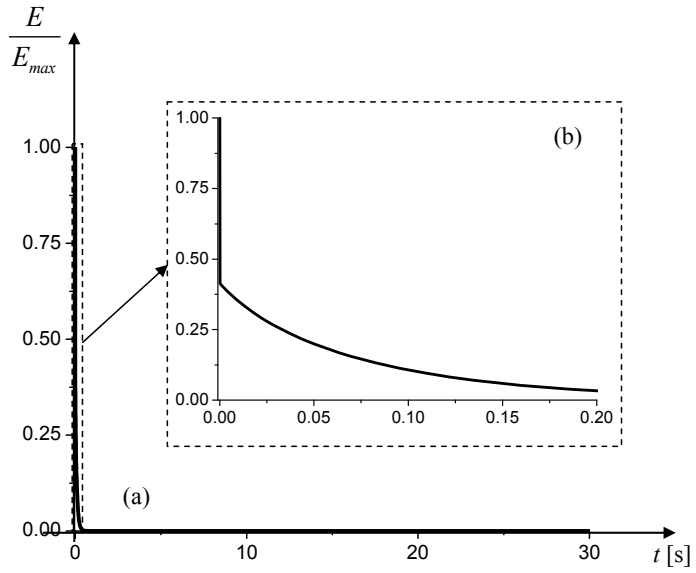

Figure 21. Charge decay plot for nonwoven fabric with a thickness of 1.80 mm at $\sigma_1 = 1 \times 10^{-9}$ S/m and $\sigma_2 = 17,500$ S/m (result of simulation); (**a**) the full scale; (**b**) the zoomed initial part of the plot.

As mentioned in Section 2, in the case of homogeneous textiles, the charge decay plots are described by Equation (1), which can be rewritten in the following form:

$$\frac{E}{E_{max}} = \mathrm{e}^{-t/\tau}, \tag{3}$$

where $\tau = RC$ is a time constant. For example, in the case of the plot shown in Figure 7d, using a program that fits the parameters of the exponential curve to the points found during simulation, $\tau = 21.63$ s is determined. The coefficient of determination, or R^2, which provides information about a model's goodness of fit, equals 0.9999, indicating a very good curve fit.

Due to the system's non-stationarity, the description of heterogeneous textiles is much more complicated. The results of many fitting attempts lead to the following conclusions. Two steps must be performed to determine the fitting curve. The first determines the fitting of the fast-change part of the characteristic, followed by the slow-change part. Such an approach yields a value of $R^2 > 0.99$. The equation

$$\frac{E}{E_{max}} = A_0 + A_1 \times \mathrm{e}^{-t/\tau_1} + A_2 \times \mathrm{e}^{-t/\tau_2} + A_3 \times \mathrm{e}^{-t/\tau_3} \tag{4}$$

approximates the plot, where τ_1 and τ_2 are related to the fast-change part of the plot and τ_3 is related to the slow-change part. To illustrate the approach, 1.8 mm thick nonwoven fabric with $\sigma_1 = 3 \times 10^{-11}$ S/m and $\sigma_2 = 10,000$ S/m is considered in detail (see Figure 9a at $\sigma_1 = 3 \times 10^{-11}$ S/m). Figure 22 shows the plot of the fast-change part of the plot.

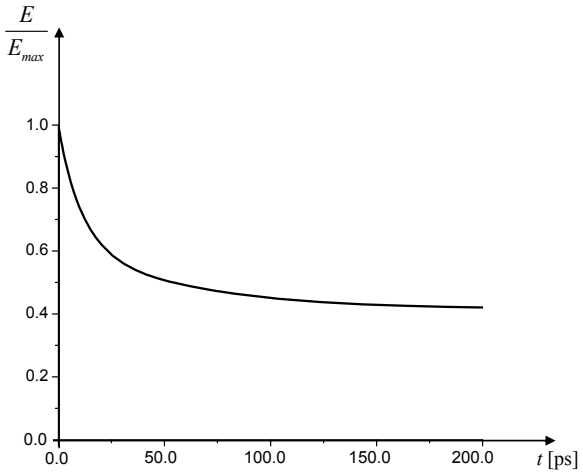

Figure 22. Fast-change part of charge decay plot at $\sigma_1 = 3 \times 10^{-11}$ S/m and $\sigma_2 = 10,000$ S/m (result of simulation).

As a result of fitting this part of the plot, $A_1 = 0.351$, $\tau_1 = 9.95$ ps, $A_2 = 0.233$, and $\tau_2 = 52.3$ ps ($R^2 = 1$) are determined. Moreover, a constant value (0.4156) is found. In the second stage, the constant is replaced by the description of the slow-change part of the charge decay plot. The parameters for fitting the second part of the plot are $A_3 = 0.384$, $\tau_2 = 2.34$ s, and a constant of 0.0042 ($R^2 = 0.9980$). After elementary manipulations, the final approximation is found as follows:

$$\frac{E}{E_{max}} = 0.032 + 0.351 \times \mathrm{e}^{-t/9.95\times10^{-12}} + 0.233 \times \mathrm{e}^{-t/52.3\times10^{-12}} + 0.384 \times \mathrm{e}^{-t/2.34}. \quad (5)$$

Figure 23 shows the original plot obtained by simulation (black dots) and the plot corresponding to the obtained approximation (solid blue line). Table 2 presents the determined values of the τ_1, τ_2, and τ_3 parameters of approximation (4) for $\sigma_1 = 3 \times 10^{-11}$ S/m and different values of σ_2. In Table 2, the results demonstrate an almost linear relationship of τ_1 and τ_2 with σ_2. A tenfold increase in σ_2 leads to a proportional decrease in τ_1 and τ_2. However, τ_3 shows a slight decrease with an increase in σ_2. When comparing the value of τ_3 with the time constant (τ) of a homogeneous material with the same σ_1, it becomes apparent that using a 25 mm × 25 mm grid of conductive fibers causes the charge to dissipate approximately 8.5 times faster than in a homogeneous textile.

Table 2. The values of the τ_1, τ_2, and τ_3 parameters of approximation (4).

σ_1 S/m	σ_2 S/m	τ_1 s	τ_2 s	τ_3 s
3×10^{-11}	0.0001	940 µ	4.55 m	2.64
3×10^{-11}	0.01	9.71 µ	50.4 µ	2.61
3×10^{-11}	1	98.5 n	525.7 n	2.62
3×10^{-11}	10	9.85 n	52.5 n	2.57
3×10^{-11}	100	985 p	5.25 n	2.47
3×10^{-11}	10000	9.95 p	52.3 p	2.34

The proposed modeling approach makes it possible to observe the effects of different damage to the specimen structure on the charge decay plot and shielding characteristics. To illustrate these possibilities, damage in the shape of a 40 mm long and 10 mm wide tear is considered. The damage leads to a break in three conductive threads (Figure 24a). Figure 24b,c show slices in the $y - z$ plane, demonstrating the effect of this damage on the values of the electric field norm. Figure 25 shows the charge decay plots for the textile before and after the damage. A significant shift between the plots can be observed.

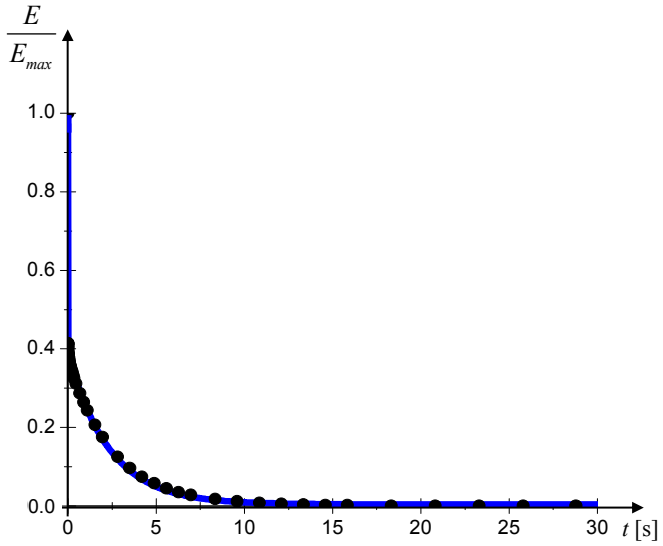

Figure 23. Original characteristics obtained by simulation (black dots) and the graph corresponding to the obtained approximation (solid blue line).

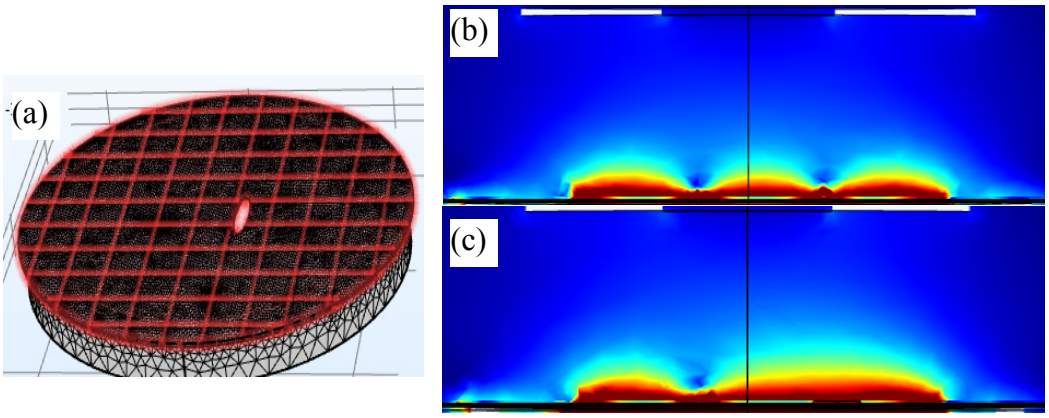

Figure 24. A specimen of nonwoven fabric (thickness of 1.80 mm with $\sigma_1 = 1 \times 10^{-11}$ S/m and $\sigma_2 = 0.01$ S/m). (**a**) Mesh with marked damage; (**b**) slice in the $y - z$ plane for t =1 µs before the damage; (**c**) slice in the $y - z$ plane for t =1 µs after the damage.

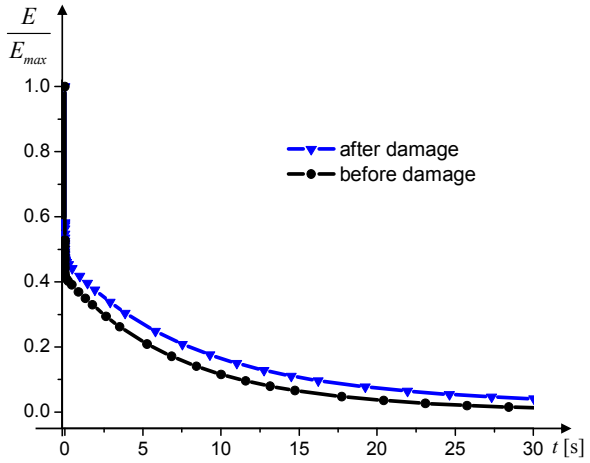

Figure 25. Charge decay plots for nonwoven fabric with a thickness of 1.80 mm at $\sigma_1 = 1 \times 10^{-11}$ S/m and $\sigma_2 = 0.01$ S/m before (black line) and after textile damage (blue line) (result of simulation).

5. Conclusions

Electrostatic discharge (ESD) protection is crucial in many industries and everyday life. The described modeling process can help in the design process of ESD protective textiles. Numerous plots and slices obtained by simulation allow for a better understanding of the charge decay phenomenon occurring in various textiles. A mathematical description of the numerically obtained plots in heterogeneous textiles with conductive grids is proposed, leading to a coefficient of determination of $R^2 > 0.995$.

During laboratory tests conducted according to the EN 1149-3 standard, the initial peak is typically significantly lower than one. The minimum technical requirements specified in the EN 1149-3 standard (sampling the measurement signal from the charge amplifier every 50 µs) result in the initial part of the charge decay plot for some ESD protection materials usually not being accurately recorded, as shown in Figures 20 and 21. Increasing the sampling frequency and amplifier bandwidth would allow the initial part of the charge decay plot to be correctly recorded. However, very high sampling frequencies of tens of GHz and advanced amplifiers would be required to capture some of the waveforms.

Laboratory tests confirm the validity of the considerations, particularly the significant influence of textile finishing treatment (firing and impregnation) on the shape of the charge decay plots and the electrostatic shielding value (S). The actual climatic conditions (especially humidity) affect the shape of the plots and the value of S. As humidity increases, the value of S also increases. Simulation studies and laboratory tests confirm that a dense grid (5 mm × 5 mm) allows us to obtain $S = 0.98$.

Author Contributions: Conceptualization, S.H. and B.W.-H.; methodology, S.H. and B.W.-H.; software, S.H. and P.S.; validation, B.W.-H.; formal analysis, S.H. and B.W.-H.; investigation, S.H. and B.W.-H.; resources, P.S. and B.W.-H.; data curation, B.W.-H.; writing—original draft preparation, S.H.; writing—review and editing, S.H., P.S., and B.W.-H.; visualization, S.H. All authors have read and agreed to the published version of the manuscript.

Funding: This research received no external funding.

Institutional Review Board Statement: Not applicable.

Informed Consent Statement: Not applicable.

Data Availability Statement: Dataset available on request from the authors.

Conflicts of Interest: The authors declare no conflicts of interest.

References

1. Bhattacharya, S.; Amin, H. Analysis of surface resistivity behavior of conductive woven fabrics made from Copper Jari & S.S./Polyester yarns for ESD control. *Int. J. Eng. Technol.* **2015**, *2*, 1007–1012.
2. Paasi, J.; Coletti, G.; Fast, L.; Lemaire, P.; Vogel, C. ESD-protective clothing for electronics industry—A new European research project ESTAT-Garments. In Proceedings of the 6th Dresden Textile Conference, Dresden, Germany, 19–20 June 2002; pp. 1–8.
3. Deschamps, C.; Simpson, N.; Dornbusch, M. Antistatic properties of clearcoats by the use of special additives. *J. Coatings Technol. Res.* **2019**, *17*, 693–710. [CrossRef]
4. Shi, Z.; Li, C.; Lei, Z.; Yang, Y.; He, J.; Song, J. Lichtenberg figures presenting electrostatic discharge patterns at different humidity. *J. Phys. D Appl. Phys.* **2021**, *54*, 34LT01.
5. Eckhoff, R.K.; Li, G. Industrial dust explosions. A brief review. *Appl. Sci.* **2021**, *11*, 1669. [CrossRef]
6. Yin, J. Charge Conduction and Dissipation in Fibers and Felts: Study by Scanning Probe Microscopy. Available online: http://hdl.handle.net/2078.1/182154 (accessed on 1 July 2024).
7. Marciniak, K.; Grabowska, K.; Stempien, Z.; Ciesielska, I.; Rutkowska, A.; Taranek, D. Woven fabrics containing hybrid yarns for shielding electromagnetic radiation. *Fibres Text. East. Eur.* **2016**, *24*, 6–109. [CrossRef]
8. Zeng, W.; Shu, L.; Li, Q.; Chen, S.; Wang, F.; Tao, X.M. Fiber-based wearable electronics: A review of materials, fabrication, devices, and applications. *Adv. Mater.* **2014**, *26*, 5310–5336. [CrossRef] [PubMed]
9. Tseghai, G.B.; Malengier, B.; Fante, K.A.; Nigusse, A.B.; Van Langenhove, L. Integration of conductive materials with textile structures, an overview. *Sensors* **2020**, *20*, 6910. [CrossRef]
10. Repon, M.R.; Mikucionien, D. Progress in flexible electronic textile for heating application: A critical review. *Materials* **2021**, *14*, 6540. [CrossRef]
11. Krifa, M. Electrically conductive textile materials-application in flexible sensors and antennas. *Textiles* **2021**, *1*, 239–257. [CrossRef]

12. Simegnaw, A.A.; Malengier, B.; Tadesse, M.G.; Van Langenhove, L. Development of stainless steel yarn with embedded surface mounted light emitting diodes. *Materials* **2022**, *15*, 2892. [CrossRef]
13. Caya, M.V.; Yrureta, R.; Chung, W.Y.; Payag, Z. Development of conductive thread heating element on wireless heating e-textile belt for thermotherapy application. *Automatika* **2021**, *62*, 293–299. [CrossRef]
14. Warska, M.; Barburski, M.; van Langenhove, L. Textile elements for car seat to improve users driving comfort. *J. Ind. Text.* **2021**, *51*, 513–539. [CrossRef]
15. Bajaj, P.; Gupta, A.; Ojha, N. Antistatic and hydrophilic synthetic fibers: A critique. *J. Macromol. Sci. Part C Polym. Rev.* **2007**, *40*, 105–138. [CrossRef]
16. Hufenus, R.; Gooneie, A.; Sebastian, T.; Simonetti, P.; Geiger, A.; Parida, D.; Bender, K.; Schach, G.; Clemens, F. Antistatic fibers for high-visibility workwear: Challenges of melt-spinning industrial fibers. *Materials* **2020**, *13*, 2645. [CrossRef]
17. Cheng, K.; Lee, K. Electrostatic discharge properties of knitted copper wire/glass fiber fabric reinforced polypropylene composites. *Polym. Compos.* **2001**, *22*, 185–196. [CrossRef]
18. Hebeish, A.; El-Gamal, M.; Said, T.; Abd El-Hady, R. Major factors affecting the performance of ESD-protective fabrics. *J. Text. Inst.* **2010**, *101*, 389–398. [CrossRef]
19. Shyr, T.W.; Lien, C.H.; Lin, A.J. Coexisting antistatic and water-repellent properties of polyester fabric. *Text. Res. J.* **2011**, *81*, 254–263. [CrossRef]
20. Hakeim, O.; El-Zawahry, M.; Aly, N.; Hawary, N.; Diab, H.; Ali, M. Anti-static and functional properties of asminosilsesquioxane oligomer treated and dyed fabrics. *J. Text. Assoc.* **2015**, *76*, 90–101.
21. Huang, L.; Xiao, L.; Kaka, G. Chitosan Application in Textile Processing. *Curr. Trends Fash. Technol. Text. Eng.* **2018**, *4*, 32–34. [CrossRef]
22. Wang, Z.; Wang, D.; Fang, Y.; Shen, J. Preparation and properties of antistatic polyethylene film coated polypropylene non-woven fabrics. *Fibers Polym.* **2018**, *19*, 934–940.
23. Chatterjee, K.; Tabor, J.; Ghosh, T.K. Electrically conductive coatings for fiber-based e-textiles. *Fibers* **2019**, *7*, 51. [CrossRef]
24. Fast, L.; Borjesson, A. Performance of Inhabited ESD-Garments and Their Interaction with Sensitive Devices. Available online: https://www.diva-portal.org/smash/get/diva2:962302/FULLTEXT01.pdf (accessed on 1 July 2024).
25. Neruda, M.; Vojtech, L. Verification of surface conductance model of textile materials. *J. Appl. Res. Technol.* **2012**, *10*, 578–584. [CrossRef]
26. Kacprzyk, R.; Król, J.; Pelesz, A. Energy stored in the electric field produced by a charged fabric with a conductive mesh. *Fibres Text. East. Eur.* **2018**, *130*, 52–58. [CrossRef]
27. Hałgas, S.; Wilbik-Hałgas, B. Some aspects of modelling and design of ESD protective fabrics. *Prz. Elektrotechniczny* **2023**, *99*, 202–206. [CrossRef]
28. Fast, L.; Franzon, J.; Mannikoff, A.; Borjesson, A. Studies on Electrical Safety, When Using ESD Protective Equipment, Especially ESD Protective Garments. Available online: http://www.diva-portal.se/smash/get/diva2:962301/FULLTEXT01.pdf (accessed on 1 July 2024).
29. Varnaitė-Žuravliova, S.; Katunskis, J. Influence of washing on the electric charge decay of fabrics with conductive yarns. *Fibres Text. East. Eur.* **2009**, *17*, 69–75.
30. Zilinskas, P.; Lozovski, T.; Jankauskas, V.; Jurksus, J. Electrostatic properties and characterization of textile materials affected by ion flux. *Mater. Sci.* **2013**, *19*, 61–66. [CrossRef]
31. Telipan, G.; Ignat, M.; Catanescu, L.; Moasa, B. Electrostatic discharge testing of several ESD protective textiles used in electronic industry. In Proceedings of the 2014 International Conference and Exposition on Electrical and Power Engineering (EPE), Iasi, Romania, 16–18 October 2014; pp. 602–605. [CrossRef]
32. Mohamad, G.A.; Shahba, A.F. Assessment of the electrostatic propensity of PES/metallic woven fabrics. *Int. J. Adv. Res. Sci. Eng.* **2015**, *4*, 1–6.
33. Perumalraj, R. Characterization of electrostatic discharge properties of woven fabrics. *J. Text. Sci. Eng.* **2016**, *6*, 1000235. [CrossRef]
34. Salceanu, A.; Iacobescu, F.; Paulet, M.; Anghel, M.A. Approach on measuring the surface resistivity of ESD-fabrics. In Proceedings of the XXI IMEKO World Congress, Measurement in Research and Industry, Prague, Czech Republic, 30 August–4 September 2015; pp. 1–8.
35. Akbarov, R.D.; Baymuratov, B.H.; Akbarov, D.N.; Ilhamova, M. Investigation of the electrical characteristics of electrically conducting yarns and fabrics. *IOP Conf. Ser. Mater. Sci. Eng.* **2017**, *254*, 072028. [CrossRef]
36. Telipan, G.; Moasa, B.; Helerea, E.; Carpus, E.; Scarlat, R.; Enache, G. ESD knitted fabrics from conductive yarns used as protective garment for electronic industry. In *Textiles for Advanced Applications*; Kumar, B., Thakur, S., Eds.; IntechOpen: Rijeka, Croatia, 2017; Chapter 14. [CrossRef]
37. Tokarska, M. Characterization of electro-conductive textile materials by its biaxial anisotropy coefficient and resistivity. *J. Mater. Sci. Mater. Electron.* **2019**, *30*, 4093–4103.
38. Asfand, N.; Daukantiene, V. *Influence of Treatment on the Bending Behaviour of Antistatic Textiles*; Sciendo: Warsaw, Poland, 2022; pp. 17–21. [CrossRef]
39. Asfand, N.; Basra, S.; Daukantiene, V.; Jamshaid, H.; Ali, Z. Influence of antistatic polyster fibers on the properties of cotton and polyester single jersey knitted fabrics. *Fibres Text.* **2022**, *29*, 10–16. [CrossRef]

40. Varnaitė-Žuravliova, S. *The Types, Properties, and Applications of Conductive Textiles*; Cambridge Scholars Publishing: Newcastle upon Tyne, UK, 2019.
41. Conductive Materials. Meet the Materials. Available online: https://www.kobakant.at/DIY/?p=8012 (accessed on 1 July 2024).
42. COMSOL Multiphysics Software. Available online: https://www.comsol.com/ (accessed on 1 July 2024).
43. *EN 1149-3:2004*; Protective Clothing—Electrostatic Properties—Part 3: Test Methods for Measuring of Charge Decay. European Committee for Standardization: Brussels, Belgium, 2004. Available online: https://www.en-standard.eu/bs-en-1149-3-2004-protective-clothing-electrostatic-properties-test-methods-for-measurement-of-charge-decay/ (accessed on 1 July 2024).
44. *EN 1149-1:2006*; Protective Clothing—Electrostatic Properties—Part 1: Test Method for Measurement of Surface Resistivity. European Committee for Standardization: Brussels, Belgium, 2006.
45. *EN 1149-2:1997*; Protective Clothing—Electrostatic Properties—Part 2: Test Method for Measurement of the Electrical Resistance through a Material (Vertical Resistance). European Committee for Standardization: Brussels, Belgium, 1997.
46. Paasi, J.; Kalliohaka, T.; Luoma, T.; Soininen, M.; Salmela, H.; Nurmi, S.; Coletti, G.; Guastavino, F.; Fast, L.; Nilsson, A.; et al. Evaluation of Existing Test Methods for ESD Garments. Available online: http://virtual.vtt.fi/virtual/estat/publications/vtt_btuo45-041224.pdf (accessed on 1 July 2024).
47. Chabay, R.; Sherwood, B. *Matter and Interactions*; Wiley: Hoboken, NJ, USA, 2015; Volume 2.
48. Vogel, C.; Beier, H.; Erth, H. Research and development in the field of special protective clothing; Requirements for selected methods and products. *Fibres Text. East. Eur.* **2006**, *14*, 29–34.
49. Ansys HFSS. Available online: https://www.ansys.com/products/electronics/ansys-hfss (accessed on 1 July 2024).
50. CST Studio Suite. Available online: https://www.3ds.com/products-services/simulia/products/cst-studio-suite/ (accessed on 1 July 2024).

Disclaimer/Publisher's Note: The statements, opinions and data contained in all publications are solely those of the individual author(s) and contributor(s) and not of MDPI and/or the editor(s). MDPI and/or the editor(s) disclaim responsibility for any injury to people or property resulting from any ideas, methods, instructions or products referred to in the content.